AGU PUBLICATIONS

JGR

Journal of Geophysical Research: Space Physics

TECHNICAL REPORTS: METHODS

10.1002/2015JA022020

Key Points:
- A technique to identify the lobe using solely magnetometer data is outlined
- Our technique is compared to a previous technique and found to identify more data in the lobe
- Our technique also yields intervals which are at least triple the length at the 90th percentile

Correspondence to:
J. C. Coxon,
work@johncoxon.co.uk

Citation:
Coxon, J. C., C. M. Jackman, M. P. Freeman, C. Forsyth, and I. J. Rae (2016), Identifying the magnetotail lobes with Cluster magnetometer data, *J. Geophys. Res. Space Physics*, *121*, doi:10.1002/2015JA022020.

Received 9 OCT 2015
Accepted 21 JAN 2016
Accepted article online 28 JAN 2016

Identifying the magnetotail lobes with Cluster magnetometer data

J. C. Coxon[1], C. M. Jackman[1], M. P. Freeman[2], C. Forsyth[3], and I. J. Rae[3]

[1]School of Physics and Astronomy, University of Southampton, Southampton, UK, [2]British Antarctic Survey, High Cross, Cambridge, UK, [3]UCL Mullard Space Science Laboratory, Holmbury St. Mary, Dorking, UK

Abstract We describe a novel method for identifying times when a spacecraft is in Earth's magnetotail lobes solely using magnetometer data. We propose that lobe intervals can be well identified as times when the magnetic field is strong and relatively invariant, defined using thresholds in the magnitude of B_X and the standard deviation σ of the magnetic field magnitude. Using data from the Cluster spacecraft at downtail distances greater than 8 R_E during 2001–2009, we find that thresholds of 30 nT and 3.5 nT, respectively, optimize agreement with a previous, independently derived lobe identification method that used both magnetic and plasma data over the same interval. Specifically, our method has a moderately high accuracy (66%) and a low probability of false detection (11%) in comparison to the other method. Furthermore, our method identifies the lobe on many other occasions when the previous method was unable to make any identification and yields longer continuous intervals in the lobe than the previous method, with intervals at the 90th percentile being triple the length. Our method also allows for analyses of the lobes outside the time span of the previous method.

1. Introduction

Stretching upward of 1000 R_E (6,371,000 km) beyond Earth [*Dungey*, 1965], the magnetotail contains two main regions: the plasma sheet and the magnetotail lobes. The plasma sheet is on closed magnetic field lines (i.e., both ends intersecting the Earth), comprises hot plasma, and contains the cross-tail current sheet. The lobes are north and south of the plasma sheet and contain open magnetic field lines (i.e., connected to Earth's polar regions at one end and to the interplanetary magnetic field (IMF) at the other). As the field lines are open, the lobes are characterized by very low density plasma and by a relatively strong and stable magnetic field, directed toward Earth ($B_X > 0$ nT) in the northern lobe and away from Earth in the southern lobe. The plasma sheet and the lobes are separated by the plasma sheet boundary layer (PSBL), comprising newly closed magnetic field lines which are pulled toward Earth due to magnetic tension, eventually becoming part of the plasma sheet [*Hughes*, 1995]. $|B_X|$ increases with distance from the plasma sheet, such that $|B_X|$ in the plasma sheet and PSBL is less than in the lobes. The broad structure of the magnetotail was first observed by *Ness* [1965].

In the Dungey cycle [*Dungey*, 1961], magnetic field lines are opened by dayside reconnection and stretched antisunward by the solar wind, forming the magnetotail lobes, before being closed again via nightside reconnection in the magnetotail and returning to the dayside where reconnection can again occur, completing the cycle. On timescales of the order of an hour, the reconnection rates on the dayside and nightside are unbalanced, giving rise to the substorm cycle in which magnetic energy [*Perreault and Akasofu*, 1978] and open magnetic flux [*Cowley and Lockwood*, 1992] are built up (when the dayside reconnection rate is larger than the nightside) and released (vice versa) [e.g., *McPherron et al.*, 1973; *Freeman and Morley*, 2009]. In order to understand this process, it is desirable to measure the magnetic field in the magnetotail lobes throughout the substorm cycle.

There are relatively few quantitative definitions of the lobes. For example, *Fairfield and Jones* [1996] simply identified the lobes as magnetotail regions north and south of two curves in the *Y*-*Z* plane (approximately $|Z| \geq 6\,R_E$ where $|Y| \leq 5\,R_E$, increasing to $|Z| \geq 12.5\,R_E$ where $|Y| = 27.5\,R_E$). A more sophisticated method was employed by *Boakes et al.* [2014, hereafter B14], who defined the lobe as the region where the plasma beta β is less than some threshold, which was determined from a decrease in the gradient of the plasma density with β. The low-β lobe region was shown statistically to correspond to noise-level currents as derived from

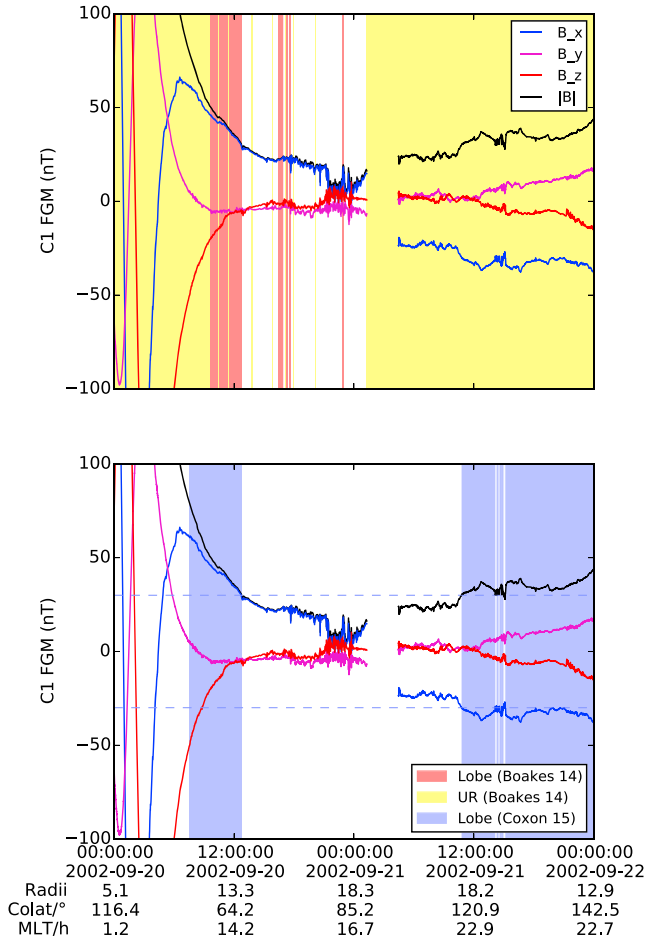

Figure 1. FGM data from Cluster 1 between midnight on 20 September 2002 and midnight on 22 September 2002. In both panels, the four curves show the GSE *X* (blue), *Y* (purple), and *Z* (red) components and the magnitude (black) of the magnetic field. (top) Color shading indicates the regions identified as lobe by the B14 method in red and as unknown in yellow. (bottom) Color shading indicates the regions identified as lobe by our method in blue.

the curlometer technique [*Dunlop et al.*, 2002]. The β threshold determined by B14 varied with time, in part, due to the changing availability and quality of the Cluster plasma instruments [*Rème et al.*, 2001]. Additionally, most of the plasma measurements were made with the Hot Ion Analyser (HIA), which has a lower density limit of 0.01 cm^{-3} such that the lobe would be unidentified when the plasma density was below that limit.

Finally, another method of identifying the lobe was proposed by *Jackman and Arridge* [2011], who identified the lobes at Saturn by looking for a relatively strong and stable magnetic field at times of relatively low plasma density compared to the plasma sheet. In this paper, we develop a new lobe identification method based on *Jackman and Arridge* [2011], using solely magnetometer data. We quantify the accuracy of our method by comparison with the identifications of the B14 method. In this way, we are able to accurately identify the magnetotail lobes without the necessity for reliable plasma measurements in this low-density region of the magnetosphere.

2. Sources of Data

The Cluster mission is comprised of four spacecraft (C1–C4) which were launched into elliptical polar orbits in July and August 2000, with a perigee of ~4 R_E and an apogee of ~19.5 R_E [*Escoubet et al.*, 1997]. Data are available from 2001 onward and taken from the Cluster Science Archive [*Laakso et al.*, 2010]. In this paper, we use fluxgate magnetometer data (FGM) [*Balogh et al.*, 2001] at spin resolution (~4 s).

The B14 method identified the magnetotail lobe using data from the Cluster spacecraft between 2001 and 2009 as part of the European Cluster Assimilation Technology (ECLAT) project. As previously mentioned,

the lobes were identified as regions where the plasma β is less than some threshold which changes in each year (of order $\beta < 0.025$). The magnetotail lobe identification was not performed for the entirety of each year; rather, only during "tail seasons," which were defined as July–October in each year. Regions were only identified where the spacecraft was judged to be well within the magnetotail (defined as $X < -8\,R_E$ and $|Y| < 15\,R_E$).

Two days of data from C1 are shown in Figure 1 (top), with the lobe intervals identified by the B14 method shaded in red. The B14 method identifies C1 in the lobe between 09:32 and 12:44 UT on 20 September 2002 (hereafter called interval 1), before C1 enters the plasma sheet. According to the B14 method, C1 encountered lobe-like characteristics twice while crossing the plasma sheet: between 16:25 and 17:39 UT (interval 2) and between 22:53 and 22:59 UT (interval 3), both on 20 September 2002.

Gaps in the identification are observed in each of the three lobe intervals outlined above. Analysis shows that two gaps of ~1 min are present in interval 1, splitting the interval into three subintervals. The larger data gaps in interval 2 can be seen by eye, but both intervals 2 and 3 are also interrupted by ~1 min gaps. More importantly, the orbit of Cluster during this time should mean that the spacecraft experiences a lobe interval after encountering the plasma sheet, but the interval after 01:00 UT on 21 September 2002 is defined as unidentified by the B14 method (which is shown in yellow). This is likely due to low plasma density impeding measurement of β, and it demonstrates the utility of the development of an identification method independent of plasma density.

3. Method: Identifying the Lobe Solely From FGM Data

We propose an alternative method of lobe identification based on FGM data alone, similar to that of *Jackman and Arridge* [2011], using the following four criteria. X_{GSE} is the sunward component of the spacecraft position in geocentric solar ecliptic (GSE) coordinates, σ is the standard deviation of the magnitude of the magnetic field for 20 min on either side of each datum (i.e., a 40 min sliding window), and $|B_X|$ is the magnitude of the sunward component of the magnetic field in GSE coordinates.

1. $X_{\mathrm{GSE}} < 0R_E$
2. Radial distance to Earth $R \geq 8R_E$
3. $\sigma \leq \sigma_0$
4. $|B_X| \geq B_0$

The first criterion ensures that the spacecraft is on the nightside of the Earth, and the second criterion ensures that the inner magnetosphere is not identified as the lobe. The third and fourth criteria are designed to identify the strong and relatively invariant magnetic field characteristic of the lobes.

Figure 1 (bottom) shows the lobe intervals in blue defined using our method with $\sigma_0 = 3.5$ nT and $B_0 = 30$ nT. Three differences between Figures 1 (top) and 1 (bottom) should be highlighted. First, interval 1 has been successfully identified and extended, starting at 07:30 and ending at 12:43 UT (with one gap in the last minute of the interval).

Second, intervals 2 and 3 are not identified by our method because $|B_X|$ falls well below the required threshold (shown by the horizontal dashed lines in Figure 1 (bottom)). It is possible that these intervals are a result of current sheet flapping while C1 was in the boundary layer between lobe and plasma sheet [*Davey et al.*, 2012]. To identify these intervals as lobe, both criteria would need to be relaxed, which would increase the probability of false detection (POFD).

Third, the lobe interval which was expected after the plasma sheet crossing (which was unidentified by the B14 method) is identified by our method on 21 September 2002, starting at 10:46 UT and continuing to 14:07 UT. There are then sporadic identifications until an uninterrupted interval starts at 15:09 UT and lasts until 04:06 UT on 22 September (beyond the range of the plot).

4. Comparison With Previous Methods

Figure 1 illustrates the main limitation of the B14 method, in that it frequently fails to return any identification. However, when the B14 method does identify the lobe, we have no a priori reason to doubt this. Consequently, we choose thresholds σ_0 and B_0 to optimize the agreement between our method and the B14 method. Figure 2 shows the occurrence frequency of $|B_X|$ and σ measured by the FGM instrument on

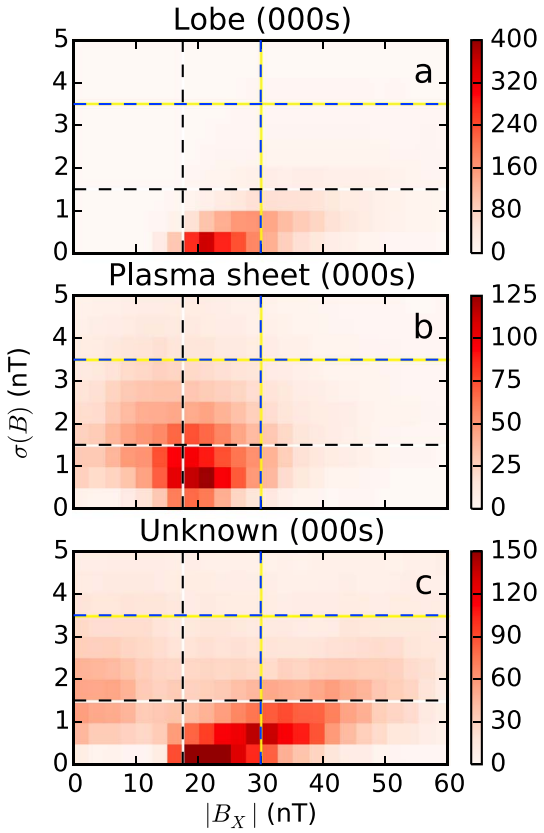

Figure 2. Occurrence of magnetotail regions identified by the B14 method as a function of $|B_X|$ and σ, with the scales in thousands of data. The regions shown are (a) the lobe, (b) the plasma sheet, and (c) the unknown region. Dashed lines indicate thresholds chosen for B_0 and σ_0 which are discussed in the text. Data from C1 are plotted from 2001 to 2009.

Cluster 1 for 2001–2009, sorted according to the corresponding region identified by the B14 method (as labeled on the plot). The bin sizes are 2.5 nT for $|B_X|$ and 0.5 nT for σ.

In Figures 2a–2c, the lobe and plasma sheet are well separated in $|B_X|$, and higher σ is observed in the plasma sheet. The thresholds $B_0 = 17.5$ nT and $\sigma_0 = 1.5$ nT are indicated by the dashed black-and-white lines and $B_0 = 30$ nT and $\sigma_0 = 3.5$ nT (the thresholds used in Figure 1, and which will be discussed in more detail later) are indicated by the dashed blue-and-yellow lines. Figure 2a shows that lobe data were identified by the B14

Table 1. Contingency Table of Lobe Identifications[a]

	ECLAT		
Coxon	Lobe	Not Lobe	Total
Lobe	3,371,826	1,246,880	4,618,706
	(2,201,930)	(2,416,776)	
Not lobe	885,694	3,426,055	4,311,749
	(2,055,590)	(2,256,159)	
Total	4,257,520	4,672,935	8,930,455

[a]A contingency table which compares the number of data which are identified as lobe by both ECLAT and our method, solely by our method, solely by ECLAT, or data which are identified as not the lobe by both methods. Data are from the tail seasons for C1 and do not include data unidentified by ECLAT. Numbers in brackets indicate the expected values given the null hypothesis that the two methods are independent. The thresholds used to generate this table were $B_0 = 7.5$ nT and $\sigma_0 = 1.5$ nT, and data are taken from 2001 to 2009. The χ^2 statistic for the table is 246,0339.

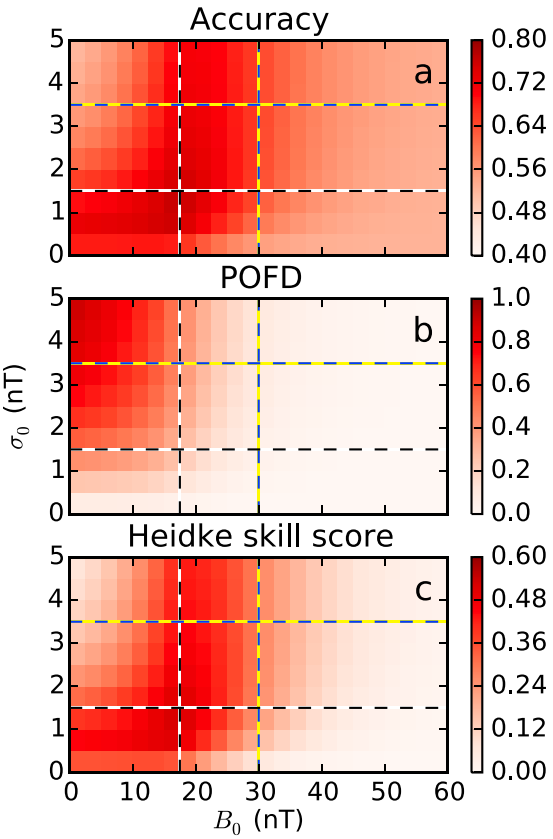

Figure 3. Variation of the measures of the agreement between our method and the B14 method as a function of thresholds B_0 and σ. (a) Accuracy, (b) the probability of false detection, and (c) the Heidke skill score (HSS). The color scale for each panel is plotted to the right of the panel; dark red indicates a larger number. Dashed lines indicate thresholds chosen for B_0 and σ_0 which are discussed in the text. Data from C1 are plotted from 2001 to 2009.

method at relatively low $|B_X|$ values, but lowering the threshold increases the probability of misidentifying plasma sheet data (Figure 2b) as lobe data.

4.1. Comparison Across the Whole Data Set

In order to decide on the thresholds of our definition of the lobes, we construct contingency tables which shows the number of data identified by each method for a given combination of B_0 and σ_0. An example is shown in Table 1 which shows data from 2001 to 2009 using thresholds of $B_0 = 17.5$ nT and $\sigma_0 = 1.5$ nT, respectively (shown as the black-and-white lines in Figure 2). Only data during the tail seasons which are positively identified by the B14 method are considered; no data labeled "unknown region" (Figure 2c) are included.

In what follows, we define a to be the number of data identified as the lobe by both our method and the B14 method (top left cell of Table 1). The number only identified by our method (top right cell) is b. The number only identified by the B14 method (bottom left cell) is c. The number not identified as the lobe by either method (bottom right cell) is d.

First, let us ask whether the two methods are related. The bracketed numbers in Table 1 are the number of data that would be expected to be in each cell given the null hypothesis that the two data sets are unrelated. For all four observing combinations the expected value (assuming independence of a given table entry) is calculated by multiplying the number of observations in the entry's row by the number in the entry's column, divided by the total number of observations in the table. Using the χ^2 statistic, the null hypothesis that the methods are independent is rejected at the 10^{-15} significance level, indicating that it is highly unlikely that the lobe identifications using the B14 method and our method are statistically different for the chosen values of B_0 and σ_0.

Given that the two methods are associated, then let us ask how well, and in what ways. From the table we see that a total of $a + d = 6,797,881$ data are identified as the same region in both lists, giving our method with these thresholds an accuracy $A = (a + d)/(a + b + c + d) = 0.76$ in reproducing the identifications from the B14 method. Using our method, we identify $b = 1,246,880$ data as lobe which the B14 method does not identify as such, corresponding to a probability of false detection $F = b/(a + d) = 0.27$ and suggesting that some of the data we identify as lobe actually exhibit boundary layer or plasma sheet characteristics. The B14 method identifies $c = 2,483,257$ data as lobe which our method does not identify, corresponding to a miss rate of $M = c/(a + c) = 0.21$, which quantifies the impact of our method's failure to identify lobe-like data according to the B14 method during plasma sheet intervals; the identification of the lobe during these intervals may also be due to movement of the plasma sheet (assuming that the identifications from the B14 method are correct). The high miss rate also gives an indication of how conservative our method is, which will be explored in more detail later.

More generally, the Heidke skill score (HSS) is given by

$$\mathrm{HSS} = \frac{2(ad - bc)}{(a + c)(c + d) + (a + b)(b + d)} \quad (1)$$

Table 2. The Best Values of B_0 and σ_0 Per Year, for $B_X > 0$ nT[a]

	B_0	σ_0	HSS	A	F
2001	25.0	2.0	0.6	0.87	0.10
2002	32.5	3.5	0.67	0.84	0.16
2003	32.5	2.5	0.53	0.81	0.15
2004	30.0	3.0	0.53	0.79	0.18
2005	32.5	4.5	0.60	0.83	0.17
2006	37.5	7.5	0.51	0.85	0.10
2007	45.0	8.0	0.51	0.91	0.03
2008	45.0	10.0	0.58	0.91	0.07
2009	50.0	8.0	0.26	0.99	0.01
Whole Range	32.5	5.0	0.55	0.81	0.16
First Half	30.0	3.5	0.58	0.81	0.18
Second Half	45.0	9.0	0.51	0.89	0.04

[a]Also tabulated are the Heidke skill score, the accuracy A, and the probability of false detection F for the two tabulated thresholds in each year.

where HSS is in the range $-\infty \leq \text{HSS} \leq 1$ and gives the relative improvement in a forecast of categorical (yes/no) observations with respect to a reference forecast. For the contingency table given in Table 1, HSS = 0.52, which shows moderate skill.

It should also be noted that in the C1 data, 2,641,497 data identified as unknown region during the tail season are now identified as the lobe by our method, with an additional 1,353,621 data identified as the lobe outside of the tail seasons. This means a total of 3,995,118 data are identified which were not previously classified by the B14 method. Added to the 4,618,706 data that were identified as lobe in Table 1, this is a total of 8,613,824 data identified as the lobe by our method. The B14 method identified 4,257,520 data as the lobe, meaning that we identify 202% the number of data that they identified with these thresholds. We cannot calculate how accurate our method is during intervals unidentified by the B14 method, but we assume that our method is at least as accurate during these times. (We note that the B14 method does not identify regions when the plasma density is very low, which is a characteristic of the lobes and may mean that our method is more accurate during unidentified intervals.)

4.2. Year-By-Year Comparison

Figure 3 shows the parameter space of B_0 and σ_0, for the time range 2001–2009, with the color scales to the right of the plots. Figure 3a shows A, Figure 3b shows F, and Figure 3c shows HSS. We define the optimal

Table 3. The Best Values of B_0 and σ_0 Per Year, for $B_X < 0$ nT[a]

	B_0	σ_0	HSS	A	F
2001	22.5	1.5	0.57	0.81	0.12
2002	27.5	3.5	0.64	0.82	0.23
2003	27.5	2.5	0.55	0.78	0.18
2004	22.5	2.0	0.59	0.79	0.23
2005	20.0	1.5	0.53	0.77	0.30
2006	20.0	1.5	0.55	0.78	0.25
2007	17.5	1.5	0.62	0.82	0.26
2008	17.5	1.5	0.55	0.78	0.34
2009	17.5	2.0	0.50	0.76	0.30
Whole range	17.5	1.5	0.53	0.77	0.30
First half	22.5	2.0	0.55	0.77	0.25
Second half	17.5	1.5	0.55	0.78	0.29

[a]Also tabulated are the Heidke skill score, the accuracy A, and the probability of false detection F for the two tabulated thresholds in each year.

Table 4. Contingency Table of Lobe Identifications[a]

	ECLAT		
Coxon	Lobe	Not Lobe	Total
Lobe	1,774,263	527,367	2,301,630
	(1,097,283)	(1,204,347)	
Not lobe	2,483,257	4,145,568	6,628,825
	(3,160,237)	(3,468,588)	
Total	4,257,520	4,672,935	8,930,455

[a]A contingency table which compares the number of data which are identified as lobe by both ECLAT and our method, solely by our method, solely by ECLAT, or data which are identified as not the lobe by both methods. Data are from the tail seasons for C1 and do not include data unidentified by ECLAT. Numbers in brackets indicate the expected values given the null hypothesis that the two methods are independent. The thresholds used to generate this table were $B_0 = 30$ nT and $\sigma_0 = 3.5$ nT, and data are taken from 2001 to 2009. The χ^2 statistic for the table is 1,075,358.

thresholds as the thresholds for which HSS is maximized, as in the previous section (for Figure 3, the optimal thresholds are $B_0 = 17.5$ nT and $\sigma_0 = 1.5$ nT).

In order to properly explore the optimal thresholds, we perform the same analysis as in Figure 3, but we filter by the sign of B_x and also do the analysis on a year-by-year basis. Positive B_X is observed in the Northern Hemisphere, and negative B_X is observed in the Southern Hemisphere. The optimal thresholds for $B_X > 0$ nT are presented in Table 2, and the thresholds for $B_X < 0$ nT are presented in Table 3. Tables 2 and 3 show that the thresholds in the magnetic field characteristics of the lobe vary with year. As such, we would recommend that for analyses of the lobe taking place during 2001–2009, the appropriate thresholds are adopted from Tables 2 and 3.

However, if analysis needs to be performed during more recent times than the B14 method, it is necessary to consider the best thresholds to use. Although the optimal thresholds from the analysis in section 4.1 are $B_0 = 17.5$ nT and $\sigma_0 = 1.5$ nT, the year-by-year list of optimal thresholds demonstrates that these thresholds may not be as accurate earlier in the mission, nor in the northern hemisphere. As such, we select more conservative thresholds for our analysis. We select thresholds of $B_0 = 30$ nT and $\sigma_0 = 3.5$ nT, based on the optimal value for 2001–2005 from Table 2, as our more conservative values. Figure 2 (yellow-and-blue lines) shows that these thresholds, while perhaps missing a number of lobe data, avoid mischaracterization of plasma sheet data as lobe data. These more conservative thresholds have an accuracy $A = 0.66$ and a Heidke skill score of 0.31, both decreases from the values quoted in section 4.1. However, the POFD decreases from 0.27 to 0.11, which is a marked improvement. The contingency table for these thresholds is shown in Table 4, and with these thresholds, 3,655,559 data are identified which were not previously classified by the B14 method. Added to the 2,301,630 data that were identified as lobe in Table 4, this is a total of 5,957,189 data, so our method identifies 140% the number of data identified by the method of B14.

Tables 2 and 3 indicate that for the majority of the time, these thresholds are either close to or more conservative than the optimal thresholds. A notable exception is the Northern Hemisphere from 2006 onward, during which time our B_0 threshold is significantly under the optimal threshold. However, we note that only 66,776 lobe data were found using the B14 method in the Northern Hemisphere in this period versus 2,150,750 in the Southern Hemisphere, such that 97% of the lobe data were located in the Southern Hemisphere during this 4 year period; we therefore conclude that the Northern Hemisphere data during this period will not have a significant effect on the results.

5. Discussion

The Cluster mission was initially launched into an elliptical polar orbit and is therefore expected to spend a lot of time in the lobes. In Figure 1 (bottom), our method identifies lobe intervals lasting 5, 4, and 13 h, consistent with these orbital characteristics. However, using both magnetic field and plasma measurements, the B14 method fails to identify the lobe in the latter part of the interval where we would expect it, in contrast

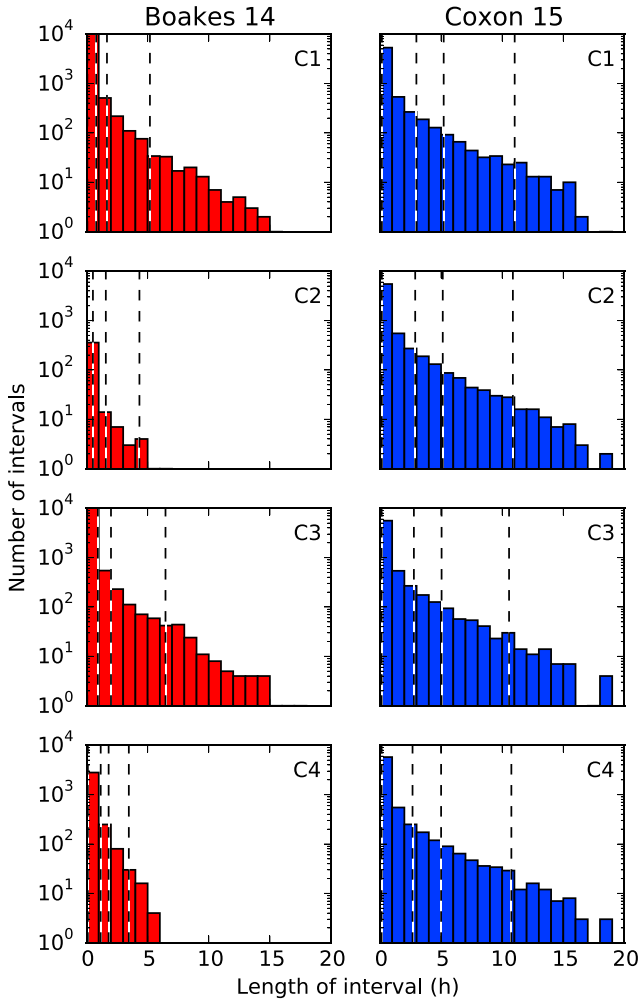

Figure 4. Histograms of the identified duration of lobe intervals by (left column) the B14 method and (right column) our method. Intervals lasting less than 1 min have been omitted. In each panel, black-and-white dashed lines show the 50th, 90th, 95th, and 99th percentiles from left to right. From top to bottom, data from C1 to C4 are plotted from 2001 to 2009.

to the successful identification from our method. As a result, while the use of the B14 method where an identification has been made is recommended, we have successfully provided a method which is able to make identifications in places where the B14 method cannot.

To examine the difference between our method and the B14 method further, Figure 4 compares the duration of lobe intervals identified by the B14 method and by our method for each spacecraft in 2001–2009. (We use the intervals $B_0 = 30$ nT and $\sigma_0 = 3.5$ nT, as in section 4.2. No interval that was shorter than 1 minute is included.) It can be seen that the longest intervals identified by the B14 method are no more than 15 h long for C1 and C3 and no more than 6 h for C2 and C4. This difference is likely due to instrumentation differences. Poor statistics are expected in C2, since both CODIF (the COmposition and DIstribution Function sensor) and HIA (the Hot Ion Analyser sensor) were nonoperational on that craft and the lobe was identified using PEACE data from 2001 to 2009. Furthermore, the quality of CODIF data degraded such that it was unreliable in 2003–2009; while both C1 and C3 use HIA during this period, C4 uses CODIF because the HIA instrument on that craft was nonoperational. Our method achieves intervals up to 18–19 h long, and the distributions are similar for all four spacecraft, confirming that this feature of the identifications of the B14 method arises from the plasma data.

Percentiles of the distributions in 2001–2009 further quantify this improvement. The percentiles for each spacecraft are similar, so we choose to examine C1. The median length of the intervals was 0.07 h in the B14 method and 0.16 h in our method: our method was 2.4 times longer. The 90th percentiles were 0.79 h and 3.0 h long, respectively: our method was 3.8 times longer. It can be seen from Figure 4 that a large number of

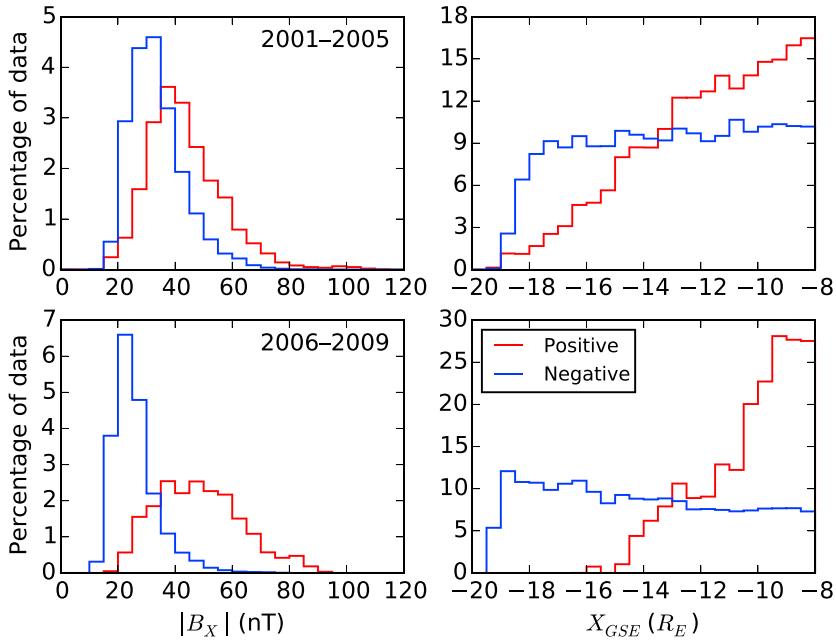

Figure 5. Percentage histograms of FGM data identified as lobe by the B14 method binned by (left column) the value of $|B_X|$ (nT) and (right column) the value of X_{GSE} (R_E). Histograms are of data from (top row) 2001–2005 and (bottom row) 2006–2009. The red (blue) line only includes data with a positive (negative) B_X.

the intervals identified in both methods are under an hour long: over 90% of intervals in the B14 method are under an hour long, compared to under 80% of intervals in our method.

In 2001–2005, the longest lobe interval identified by the B14 method was 8–9 h long; in this time frame, our longest intervals last twice as long. However, in 2006–2009, the longest intervals identified by the two methods are of comparable length, with both methods yielding maximum intervals ~15 h. The B14 method identifies more lobe data relative to the number of their identified plasma sheet data in 2006–2009, indicating that the B14 method identifies the lobe more readily in this time period.

Tables 2 and 3 indicate that the populations of the lobe identified by the B14 method exhibit generally lower values for both σ and $|B_X|$ in the Southern Hemisphere (and vice versa for the Northern Hemisphere) as the mission progresses. We attribute this to the lower values in both of the chosen magnetic field parameters. The lower $|B_X|$, as well as the larger number of identifications from the B14 method, is due to the evolving orbit of Cluster: In earlier years, the apogee was located close to $Z = 0$; i.e., it was situated in the plasma sheet. In later years, the apogee moved such that it was located at points $Z < 0$, meaning it was more often situated in the southern magnetotail lobe during the tail season. Additionally, the apogee was located at large downtail distances in the part of the lobe closest to the plasma sheet, meaning that the spacecraft spends proportionally more time in part of the lobe with weaker magnetic field.

To further investigate this point, Figure 5 shows histograms of the percentages of FGM data identified as lobe by the B14 method, binned by $|B_X|$ and X_{GSE} and subdivided by the sign of B_X (such that the Northern Hemisphere is represented by the red line and the South Hemisphere by the blue line) and by time span (2001–2005 at the top, 2006–2009 at the bottom). Looking at $|B_X|$ (Figure 5, left column), lobe data in the Northern Hemisphere are identified by the B14 method at generally higher values of $|B_X|$ than those in the Southern Hemisphere, and this effect is more pronounced later in the mission. The peak in the Northern Hemisphere is at 37.5–40.0 nT in both panels, whereas the Southern Hemisphere has a peak at 35.0–37.5 nT in 2001–2005 and a peak at 20.0–22.5 nT in 2006–2009. The radial distance of the data (Figure 5, right column) is also plotted; Southern Hemisphere lobe data are identified by the B14 method at a range of distances with a slight bias toward closer distances in 2001–2005 and toward more distant measurements in 2006–2009. The Northern Hemisphere data have a peak at $8R_E$ in both panels, with that peak being larger in 2006–2009. (The plots show the proportion of the data in each bin, so it is worth restating that there are fewer data in the Northern Hemisphere than in the South Hemisphere and this difference is extreme in 2006–2009.)

It is also possible that the difference could also be attributed to a solar cycle effect: the solar maximum of solar cycle 23 was in 2000, whereas the solar maximum in solar cycle 24 occurred well after 2009 (the exact point of maximum is still disputed). Solar cycle 23 was more active than 24, which implies that IMF penetration into the magnetosphere would have been larger earlier in the Cluster data set. This might be a component in the explanation for why the value of $|B_X|$ was greater earlier in the mission. This investigation will form the basis of a follow-up study regarding the IMF interconnection field observed in the lobes, and so we hope to shed more light on this in the future (J. C. Coxon et al., Magnetic field fall-off in the magnetotail lobes, 25th Cluster Workshop, Venice, Italy, manuscript in preparation, 2015). The average solar wind pressure was also higher during 2001–2005, which would also contribute to higher observed $|B_X|$.

6. Conclusion

We outline a novel method of identifying the magnetotail lobes purely from thresholds in spacecraft position (on the nightside, at least $8R_E$ from Earth) and magnetic field (magnitude of B_X and the standard deviation of $|B|$). In order to select the magnetic field thresholds, we explore the parameter space of varying thresholds and compare the result to identifications from the same time frame in a recent catalog of magnetotail regions derived from magnetic field and plasma measurements [*Boakes et al.*, 2014].

We report the optimal thresholds of the magnetic field by year and sign of B_X, as well as determining the most skilful thresholds to use across the entire data set, determined to be $B_0 = 17.5$ nT and $\sigma_0 = 1.5$ nT. We choose more conservative thresholds than these in order to limit the number misidentifications in the Northern Hemisphere and earlier in the mission, selecting $B_0 = 30$ nT and $\sigma_0 = 3.5$ nT. These thresholds have a Heidke skill score of 0.31, with an accuracy of 0.66 and a probability of false detection of 0.11. Although our chosen thresholds are not the most skilful thresholds for the 9 year period in both hemispheres, we argue that the much lower probability of false detection makes these thresholds more suitable, and so we adopt these thresholds as conservative thresholds of the magnetic characteristics of the lobe. We find that the number of data identified as lobe by our method during 2001–2009 is 140% the number identified by the method of B14.

Finally, our method, using the selected conservative thresholds, yields uninterrupted lobe intervals which last much longer than those of the B14 method. Specifically, the median length in our method was 0.16 h long and in the B14 method was 0.07 h long; the lengths of the 90th percentile were 2.98 and 0.79 h long, respectively. For both, our method at least tripled the length, with lengths consistent with the expected duration of lobe measurements from an elliptically polar orbiting spacecraft. This better continuity will be useful for various studies of the temporal evolution of tail properties on hour to day time scales and will be exploited by us in forthcoming studies examining both the properties of the magnetic field in the lobes and how magnetic energy is stored and released during a substorm cycle.

Acknowledgments

This work is supported by Natural Environment Research Council (NERC) joint grants NE/L007177/1 (J.C.C. and C.M.J.), NE/L006456/1 (M.P.F.), and NE/L007495/1 (C.F. and I.J.R.). Cluster data used in this paper were downloaded from the European Space Agency's Cluster and Double Star Science Archive (http://www.cosmos.esa.int/web/csa/access). We also acknowledge use of the matplotlib, NumPy, and SpacePy libraries for Python. Files used were generally of the form: (1) C*I*_CP_FGM_SPIN__*Y*0101_000000_*Y*1231_235959_V140305.cdf*, (2) C*I*_CQ_FGM_CAVF__*Y*0101_000000_*Y*1231_235959_V140305.cdf*, and (3) C*I*_CP_AUX_ECLAT_REGION__20010101_000000_20141231_235959_V131120.cdf, where $I \in \{1, 2, 3, 4\}$ and $Y \in \{2001, 2002, 2003, 2004, 2005, 2006, 2007, 2008, 2009\}$. Although most files had the version number 140305 (as above), the version number was 141122 on C1 and C2 data in 2009 and C3 data in 2006; 140724 on C1 caveats from 2009; 150121 on C3 data and caveats in 2009; and 150212 on C2 data and caveats in 2006.

References

Balogh, A., et al. (2001), The Cluster magnetic field investigation: Overview of in-flight performance and initial results, *Ann. Geophys.*, *19*(10–12), 1207–1217, doi:10.5194/angeo-19-1207-2001.

Boakes, P. D., R. Nakamura, M. Volwerk, and S. E. Milan (2014), ECLAT Cluster spacecraft magnetotail plasma region identifications (2001–2009), *Dataset Pap. Sci.*, *2014*, 684305, doi:10.1155/2014/684305.

Cowley, S. W. H., and M. Lockwood (1992), Excitation and decay of solar wind-driven flows in the magnetosphere-ionosphere system, *Ann. Geophys.*, *10*, 103–115.

Davey, E. A., M. Lester, S. E. Milan, R. C. Fear, and C. Forsyth (2012), The orientation and current density of the magnetotail current sheet: A statistical study of the effect of geomagnetic conditions, *J. Geophys. Res.*, *117*, A07217, doi:10.1029/2012JA017715.

Dungey, J. W. (1961), Interplanetary magnetic field and the auroral zones, *Phys. Rev. Lett.*, *6*, 47–48.

Dungey, J. W. (1965), The length of the magnetospheric tail, *J. Geophys. Res.*, *70*(7), 1753–1753, doi:10.1029/JZ070i007p01753.

Dunlop, M. W., A. Balogh, K.-H. Glassmeier, and P. Robert (2002), Four-point Cluster application of magnetic field analysis tools: The curlometer, *J. Geophys. Res.*, *107*(A11), 1384, doi:10.1029/2001JA005088.

Escoubet, C., R. Schmidt, and M. Goldstein (1997), Cluster—Science and mission overview, in *The Cluster and Phoenix Missions*, edited by C. P. Escoubet, C. T. Russell, and R. Schmidt, pp. 11–32, Springer, Netherlands, doi:10.1007/978-94-011-5666-0_1.

Fairfield, D. H., and J. Jones (1996), Variability of the tail lobe field strength, *J. Geophys. Res.*, *101*(A4), 7785–7791, doi:10.1029/95JA03713.

Freeman, M. P., and S. K. Morley (2009), No evidence for externally triggered substorms based on superposed epoch analysis of IMF B_z, *Geophys. Res. Lett.*, *36*, L21101, doi:10.1029/2009GL040621.

Hughes, W. J. (1995), The magnetopause, magnetotail and magnetic reconnection, in *Introduction to Space Physics*, edited by M. G. Kivelson and C. T. Russell, chap. 9, pp. 227–287, Cambridge Univ. Press, Cambridge, U. K.

Jackman, C. M., and C. S. Arridge (2011), Statistical properties of the magnetic field in the Kronian magnetotail lobes and current sheet, *J. Geophys. Res.*, *116*, A05224, doi:10.1029/2010JA015973.

Laakso, H., C. Perry, S. McCaffrey, D. Herment, A. Allen, C. Harvey, C. Escoubet, C. Gruenberger, M. Taylor, and R. Turner (2010), Cluster active archive: Overview, in *The Cluster Active Archive*, edited by H. Laakso, M. Taylor, and C. P. Escoubet, pp. 3–37, Springer, Netherlands, doi:10.1007/978-90-481-3499-1_1.

McPherron, R. L., C. T. Russell, and M. P. Aubry (1973), Satellite studies of magnetospheric substorms on August 15, 1968: 9. Phenomenological model for substorms, *J. Geophys. Res.*, *78*(16), 3131–3149, doi:10.1029/JA078i016p03131.
Ness, N. F. (1965), The Earth's magnetic tail, *J. Geophys. Res.*, *70*(13), 2989–3005, doi:10.1029/JZ070i013p02989.
Perreault, P., and S. I. Akasofu (1978), A study of geomagnetic storms, *Geophys. J. Int.*, *54*(3), 547–573, doi:10.1111/j.1365-246X.1978.tb05494.x.
Rème, H., et al. (2001), First multispacecraft ion measurements in and near the Earth's magnetosphere with the identical Cluster ion spectrometry (CIS) experiment, *Ann. Geophys.*, *19*(10–12), 1303–1354.